ELSEVIER

Earth and Planetary Science Letters 210 (2003) 579–586

EPSL

www.elsevier.com/locate/epsl

A theoretical model for reverse water-level fluctuations induced by transient permeability in thrust fault zones

Eyal Stanislavsky *, Grant Garven

Department of Earth and Planetary Sciences, Johns Hopkins University, Baltimore, MD 21218, USA

Received 6 December 2002; received in revised form 13 March 2003; accepted 14 March 2003

Abstract

A numerical model was applied to simulate the poroelastic response to changes in fault permeability as a result of earthquakes. The 'fault valve' model describes faults as impermeable barriers for fluids except immediately after earthquakes, when fault zones are damaged and transient pathways for fluids are created. In this case the fault is viewed as a discharging well, draining fluids from the surrounding rock. The reverse water-level effect is characterized by the increase of water level in adjacent aquifers and aquitards, resulting from withdrawing fluids through a well. Theoretical calculations suggest that the reverse water-level effect exists also in earthquake cycling and is in the same order of magnitude as the co-seismic hydraulic head change. A significant rise of the hydraulic head (>1 m) occurs within the country rock from both sides of the fault. The rise of the water level takes months to years to occur, and perhaps that is why it cannot be easily distinguished from seasonal hydrologic changes observed in the field. The reverse water-level effect also propagates away from the fault at a rate of hundreds of meters per year, depending on the permeability of the country rock. In deep formations where the permeability is low, the propagation takes years. The magnitude of the reverse water-level effect is greater when the fault efficiently drains fluids, when it is highly permeable and slow to reseal.

1. Introduction

The mechanical interplay between groundwater and tectonic stress is crucial for understanding the geophysical processes associated with earthquakes and the seismic cycle. Following an earthquake, changes in groundwater level and surface water discharge are well known [1,2]. Pore fluids support a part of the normal stress that is equivalent to the pressure of the fluid and act as an internal force that resists load [3]. In fault zones, increasing fluid pressure changes the fault shear strength, thereby increasing the tendency for triggering an earthquake as the strength decreases [4]. Furthermore, fault zones are thought to control fluid migration by changing their permeability during an earthquake cycle.

The 'fault valve' model describes faults as impermeable barriers for fluids except immediately after earthquakes, when fault zones are damaged and transient pathways for fluids are created [5]. When the fluids in the crust are overpressured, the faults act like a valve, draining fluid upwards be-

* Corresponding author. Tel.: +1-410-516-8543; Fax: +1-410-516-7933.
E-mail address: eyal@jhu.edu (E. Stanislavsky).

0012-821X/03/$ – see front matter © 2003 Elsevier Science B.V. All rights reserved.
doi:10.1016/S0012-821X(03)00159-6

fore the fault is resealed due to hydrothermal mineralization. A necessary condition for fault valve behavior is the presence of a laterally extensive hydrologic barrier that maintains a suprahydrostatic (overpressured) pressure gradient. Evidence of fault valve behavior was indicated by increasing post-seismic spring discharge [1,6] and petrology of ancient faults [7–9].

As a consequence of the fault permeability increase immediately after an earthquake and the subsequent drainage of fluids through the faults, the mechanical behavior of the fault is changed from undrained behavior towards drained behavior as $t \to \infty$. Thus, complex poroelastic behavior takes place when coupling the hydrological changes with the mechanical changes associated with the earthquake [10]. To explore the physical behavior of a porous medium after an earthquake, we have conducted a theoretical study where we mathematically model the medium's pore pressure and stress evolution after an earthquake, using a finite-element code for a two-dimensional, plane strain cross-section. In this model we are able to control the different hydrological and mechanical variables, which allows us to quantify each poroelastic process.

2. The reverse water-level effect

It has been observed in many field tests that when groundwater is pumped from an aquifer, the water level may momentarily increase in adjacent aquifers and aquitards [11–15]. This reverse water-level response was first observed in Noordbergum, The Netherlands, where the phenomenon earned its name for a special case where the water-level rise occurs in an aquifer separated by a confining unit from the pumped aquifer [12]. This paradoxical behavior was modeled analytically and was called the Mandel–Cryer effect [16–18]. Reverse water-level fluctuation has been modeled successively by the finite-element method for water well–aquifer interaction [19–21].

The physical explanation for this behavior rests on the time lag between stress transfer and fluid transport [12,18]. Stress transfer in a material is immediate because the deformed medium must satisfy stress compatibility. Fluid transport, however, is a diffusion-type process, and thus the fluid dissipation is time-dependent. The loss of water due to pumping involves a decrease of volume, producing radial solid displacements towards the well. The displacement field (loading solid skeleton) compensates for the loss of water. For deeper layers, this displacement field causes compression, and hence an increase of pore pressure [12]. This loading information is transferred immediately throughout the medium because of stress compatibility, but the dissipation of the pore pressure as a result of pumping requires time.

According to the fault valve model, immediately after an earthquake, fluids are channeled to the fault and discharged upwards to the surface. In this sense, the fault can be viewed as a discharge well and the reverse water-level effect may occur.

3. Model formulation and assumptions

Following Biot's [22] formulation, the force equilibrium equations can be written using solid displacements and pore pressure as the primary variables for isothermal conditions [23]:

$$G\nabla^2\underline{u} + \frac{G}{1-2\nu}\nabla(\nabla\cdot\underline{u}) = \alpha\nabla p - \underline{F} \tag{1}$$

where G is the shear modulus, $\underline{u}$ is the solid displacement vector, ν is the drained Poisson's ratio, α is Biot's coefficient, p is the pore pressure, and $\underline{F}$ is the body force. The fluid mass conservation equation for saturated isothermal flow is [23]:

$$-\nabla\cdot\left(\frac{\underline{\underline{k}}}{\mu}\nabla(p+\rho_f g z)\right) = \alpha\frac{\partial(\nabla\cdot\underline{u})}{\partial t} + S_\varepsilon\frac{\partial p}{\partial t} \tag{2}$$

where $\underline{\underline{k}}$ is the permeability tensor of the medium, μ is the fluid viscosity, ρ_f is the fluid density, g is the gravitational acceleration, and S_ε is the specific storage at constant strain. The poroelasticity equations are solved using the finite-element method for a two-dimensional, plane strain, cross-section [24], closely following the formulation of Lewis and Schrefler [19].

A generic continental domain was discretized with a mesh covering a region 75 km long and

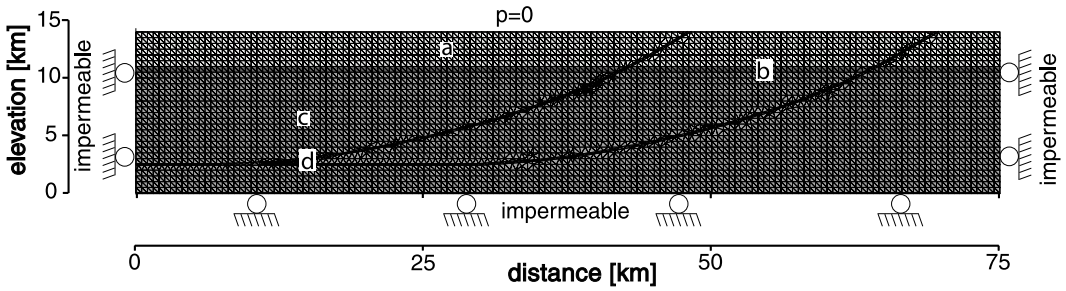

Fig. 1. Numerical mesh and boundary conditions. The lithological units include sediment layer (a), metamorphic unit (b), basement (c) and two thrust faults (d). Mechanical and hydrological properties are listed in Table 1. The hydrologic boundary conditions include $p=0$ top boundary (water table) and impermeable lower and horizontal boundaries. The mechanical boundary conditions: bottom boundary free to move horizontally and fixed vertically, right and left boundaries free to move vertically and fixed horizontally, and top boundary free to move in all directions.

14 km deep that included two very large thrust planes which cross-cut sedimentary beds and crystalline basement (Fig. 1). The assumed hydraulic and poroelastic properties are listed in Table 1.

The top boundary of the cross-section represents the land surface ($p=0$) and is open to the atmosphere. The bottom and lateral sides are assumed to be impermeable. Mechanically, the right and left boundaries are free to move vertically, but are fixed horizontally. The bottom boundary is free to move horizontally, but is fixed vertically. The top boundary is free to move vertically and horizontally.

Hubbert and Rubey [32] defined the pore-fluid factor as:

$$\lambda_V = p/\sigma_v = p/(\rho_r g z) \quad (3)$$

where σ_v is the vertical stress and ρ_r is the rock density. λ_V for hydrostatic gradients is the ratio of fluid to rock density (~ 0.4). There are abundant borehole measurements and structural rock fabrics showing that fluid pressures exceed the least principal stress ($\lambda_V = 1$) in tectonically active areas [33–36]. The transition from a hydrostatic gradient ($\lambda_V = 0.4$) to a suprahydrostatic gradient ($\lambda_V = 1$) may occur across a layer with low permeability [5]. To calculate the initial pore-pressure profile, we assumed $\lambda_V = 0.42$ for depths shallower than 2.5 km and $\lambda_V = 0.75$ for depths greater than 3 km. The numerical model was then run for 2000 yr, allowing for some dissipation of pore pressure. As a result, the pore pressure decreased everywhere in the cross-section. This newly calculated pore pressure was then used as the initial pore-pressure distribution for the simulations discussed below. The quasi-static pore-pressure

Table 1
Simulation parameters

Model properties	Sandstone[a]	Metamorphic[b]	Basement[c]	Faults[d]
Drained bulk modulus [GPa]	8	40	25	7.9
Poisson's ratio [–]	0.2	0.25	0.25	0.29
Solid bulk modulus [GPa]	36	50	45	40
Initial permeability [m^2]	$k_h = 10^{-16}$ $k_v = 10^{-18}$	$k_h = 10^{-18}$ $k_v = 10^{-19}$	$\log k_h = -14-3.2\log z$ $k_p = k_n/2$	$\log k_n = (-14-3.2\log z)/100$ $k_v = k_h/50$
Initial porosity [–]	0.19	0.02	0.01	0.01

[a] Elastic properties are of Berea sandstone [23] and hydrologic parameters are of typical sandstone [25].
[b] Elastic and hydrologic properties are of Tennessee marble [26].
[c] Elastic properties are of Westerly granite [26] and hydrologic parameters are based on compilation in [27].
[d] Elastic properties are of 70% quartz and 30% clay [28,29]. Clay parameters are from [30]. Hydrologic properties are assumed to be less than the host rock [31].

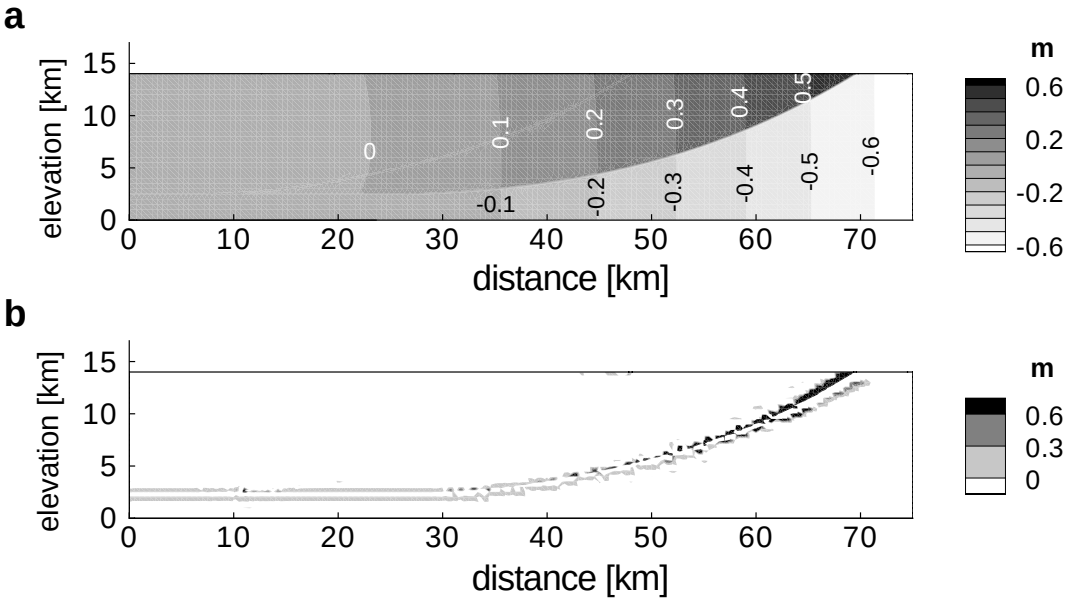

Fig. 2. (a) Hydraulic head change as a result of dislocation on the fault. The magnitude of the displacements along the fault is set to be uniform (2.0 m) and parallel to the fault plane. The changing dip of the fault is responsible for diverging displacements at the footwall (decreasing pore pressure) and converging displacements at the hanging wall (increasing pore pressure). There are no hydraulic head changes in the first 30 km because the fault is horizontal. (b) Hydraulic head increase 300 days after the permeability changes. Only positive changes are shown, so that decrease of hydraulic head due to migration of fluids to the top boundary is not shown in this figure. Significant rise of the hydraulic head occurred within the country rock on both sides of the fault.

change caused by earthquake dislocation has been successfully applied for fault-related processes [37–39]. We assumed a constant 2 m displacement along the rupturing fault. To simulate the effects of fault resealing and healing following the earthquake, the permeability of the rupturing fault was increased instantaneously by two orders of magnitude and then decreased according to a power-law equation [40]:

$$k_f = k_0 e^{-rt} \quad (4)$$

where k_0 is the fault permeability before the earthquake, the decay rate $r = 0.008$ day^{-1}, and t is time in days.

4. Results

Hydraulic head change as a result of dislocation on the fault is shown in Fig. 2a. The magnitude of the displacements along the fault is set to be uniform (2.0 m) and parallel to the fault plane. Therefore, the direction of the displacements is changing with the fault dip from 30° at the surface to 0° at 12 km depth. The changing dip of the fault is responsible for diverging displacements at the footwall (decreasing pore pressure) and converging displacements at the hanging wall (increasing pore pressure). Maximum hydraulic change is 0.6 m. There are no hydraulic head changes in the first 30 km because the fault is horizontal.

The hydraulic head increase, not including coseismic changes, is shown in Fig. 2b 300 days after the permeability changes. Only positive changes are shown, so that a decrease of hydraulic head due to migration of fluids to the top boundary is not shown in this figure. A significant rise of the hydraulic head occurred in the country rock on both sides of the fault. Prior to the simulated earthquake, the hydraulic head decreased everywhere in the cross-section. Therefore, the in-

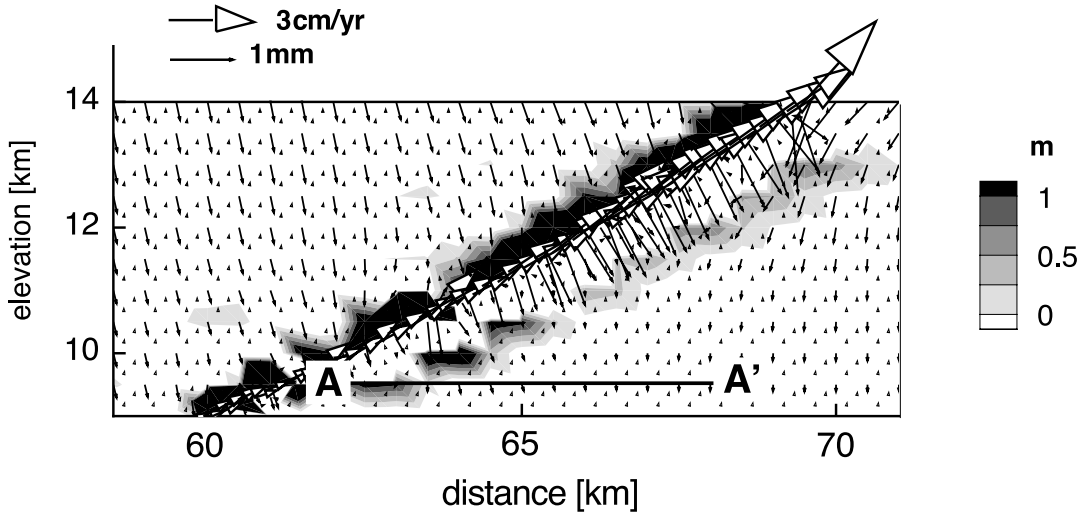

Fig. 3. Hydraulic head increase 300 days after the permeability changes at shallow depths. Rock displacements (plain arrow heads) and fluid velocities (hollow arrow heads) are also shown. The significantly high permeability within the fault zone channels fluids into the fault and up to the surface. To compensate for this fluid volume loss, the surrounding rocks are displaced toward the fault. This kind of displacement field causes loading. Elements further away from the fault are displaced but are not yet drained, resulting in an increase in hydraulic head. Hydraulic head changes along A–A′ are shown in Fig. 4.

crease of the hydraulic head within the rocks around the fault is associated with the permeability changes of the fault, and can only be explained by the reverse water-level effect (the co-seismic effects are not included in this figure). An enlargement of Fig. 2b at a shallow depth is shown in Fig. 3. Rock displacements (plain arrow heads) and pore-fluid velocities (hollow arrow heads) are also shown. The significantly high permeability within the fault zone channels fluids into the fault and up to the land surface. Fluids are diffusing into the fault from the surrounding rock and discharging upwards. The loss of fluids involves loss of bulk volume. To compensate for this volume loss, the surrounding rocks are displaced toward the fault. This kind of displacement field causes loading. Elements further away from the fault are displaced, but are not yet drained and this results in an increase in hydraulic head.

To further investigate the reverse water-level effect, one simulation was conducted on a simplified case where the permeability was increased by two orders of magnitude at the right fault, which then remained fixed at that value. The hydraulic head changes, not including the co-seismic changes, at 13 points, 500 m apart, at a depth of 4.5 km, along line A–A′ (see Fig. 3 for location) are shown in Fig. 4a. The reverse water-level effect is propagating away from the fault. As the fault drains, it also diffusively drains its neighboring elements. With time, elements further away from the fault are being drained too. The reverse water-level effect propagates at the same pace as the drainage, but one phase ahead. The propagation is primarily horizontal and not perpendicular to the fault because the horizontal permeability is two orders of magnitude greater than the vertical permeability (Table 1). However, because the fault is not vertical, the drainage of a point at the footwall can take place not only horizontally, but also vertically. Therefore, the reverse water-level effect is increasing as the front is propagating as a result of better drainage until it reaches its maximum, 2 km from the fault, after 3.5 yr. The reverse water-level effect then dissipates and after 9 yr it can no longer be observed. The rate of the maximum propagation of the reverse water-level effect increases initially to 1.5 km/yr after 8 months and then decreases gradually to 0.68 km/yr after 6 yr (Fig. 5).

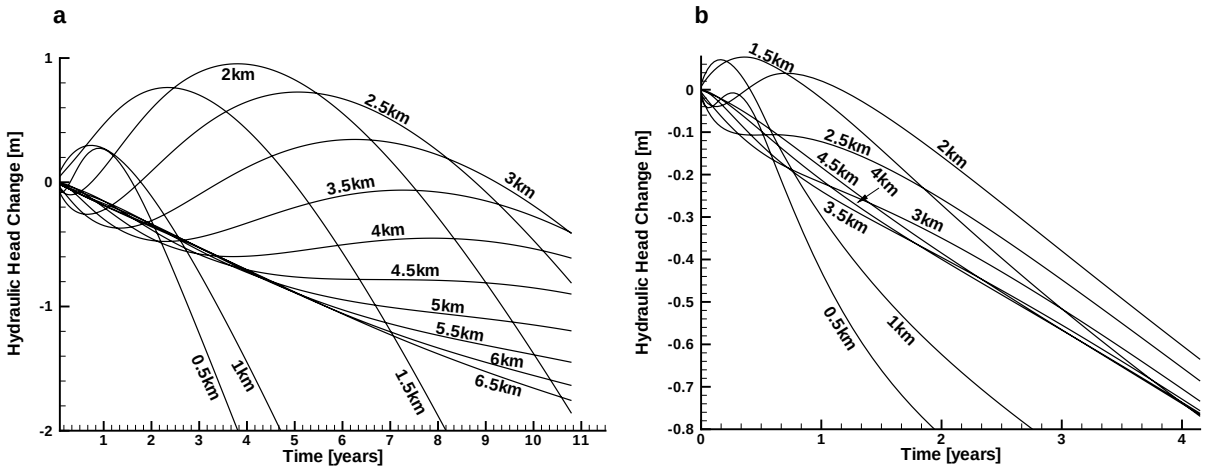

Fig. 4. Hydraulic head changes at 13 points, 500 m apart from each other, at a depth of 4.5 km, along line A–A′ (see Fig. 3 for location). (a) Permanent permeability change. The permeability is increased by two orders of magnitude and remains at the same value. The reverse water-level effect is propagating away from the fault. With time, elements further away from the fault are being drained too. The reverse water-level effect propagates at the same rate as the drainage, but one phase ahead. Because the fault is not vertical, the drainage of a point at the footwall can take place not only horizontally but also vertically. Therefore, the reverse water-level effect is increasing as the front is propagating as a result of better drainage, until it reaches its maximum after 3.5 yr, 2 km from the fault. The reverse water-level effect then dissipates and after 9 yr it can no longer be observed. (b) Fault valve permeability change. After an increase by two orders of magnitude, the fault is resealed according to Eq. 4. Both the magnitude and the rate of propagation of the reverse water-level effect are decreased because of lower efficiency of the fault to drain fluids.

The hydraulic head changes along line A–A′, when the fault is resealed according to Eq. 4, are shown in Fig. 4b. The non-linearity introduced by Eq. 4 decreases both the magnitude and the rate of propagation of the reverse water-level effect.

5. Discussion and conclusions

Co-seismic changes in pore pressure are created as a result of displacement gradient (strain) along the rupturing fault. A displacement gradient is formed by non-uniform displacement magnitude or direction. Therefore, uniform dislocation on a straight fault will not create pore-pressure changes. Most quasi-static deformation models account for non-uniform displacement magnitude, where there is stress concentration at the fault tip, but not for a non-uniform displacement direction [38,39,41]. Masterlark et al. [37] accounted for a fault with a non-uniform dip. In this work we assume a theoretical earthquake with a uniform displacement magnitude (2.0 m) and non-uniform displacement direction. A different earthquake with non-uniform displacement magnitude may cause larger hydraulic head changes.

The reverse water-level effect has been observed in many aquifer pumping tests, but has never been considered as a factor in earthquake cycling. After an earthquake, when a fault is ruptured and its permeability increased significantly, the fault can be viewed hydrologically as a pumping well,

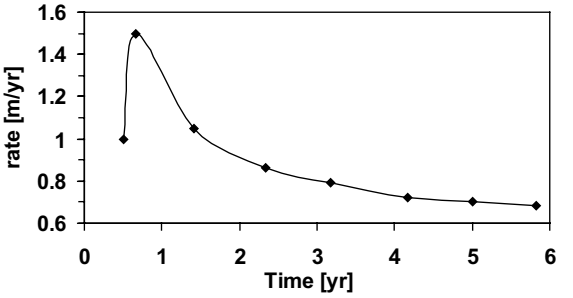

Fig. 5. The rate of the maximum reverse water-level effect propagation calculated from Fig. 4a.

draining water to the land surface. Although the fault is then resealed by mineralization, the reverse water-level effect should take place.

The velocity of the reverse water-level effect front is primarily a function of the permeability. At depths of 4.5 km (A–A′), the horizontal permeability of the rock is $10^{-16.1}$ m^2 and the reverse water-level effect front is propagating at a rate of 0.7 km/yr after 5 yr. At greater depth, the permeability is lower, which results in slower propagation of the front. The magnitude of the reverse water-level effect is greater when the fault efficiently drains fluids. Two factors controlling draining fluids are: (1) the magnitude of the fault permeability changes after rupture and (2) the rate of resealing. High permeability increase and low resealing rate imply high efficiency of the fault to drain fluids, resulting in a high magnitude of the reverse water-level effect.

The behavior of the system is a superposition of the reverse water-level effect with the poroelastic rebound of the co-seismic event. In this work we have modeled the reverse water-level effect and showed that it is in the same order of magnitude as the co-seismic water-level changes. Numerical models of earthquakes show a change of up to 10 m in the hydraulic head for big earthquakes [38]. Reverse water-level response may be more than 1 m in an extreme case where the fault is not resealing.

In this work, there is a low-permeable metamorphic layer that separates the shallow sandstone aquifer and deep water in the basement during the interseismic period. After the earthquake, during the post-seismic period, the fault is ruptured and fluids from the basement are channeled upwards through the fault. This scenario is consistent with the fault valve model [5]. However, the reverse water-level effect also occurs in a homogeneous crust.

Observed water-level changes associated with earthquakes are usually from relatively shallow wells, which are strongly influenced by seasonal changes of rainfall [2]. These shallow wells penetrate highly permeable layers in which the reverse water-level effect can propagate at rates of meters per weeks to months. Because the time scale of the seasonal changes and the reverse water-level effect is about the same, it is difficult to distinguish between them. Water-level changes from deeper wells, where seasonal changes are less significant, ought to show the reverse water-level effect more clearly.

Acknowledgements

The research reported in this paper was supported by funding from the Department of Energy (DE-FGO2-96ER14619). We appreciated the helpful discussions with Jim Rice, Renata Dmowska, and John Rudnicki. We thank the two anonymous reviewers for their comments and criticism that helped in improving the manuscript.*[RV]*

References

[1] R. Muir-Wood, G.C.P. King, Hydrological signature of earthquake strain, J. Geophys. Res. 98 (1993) 22035–22068.
[2] E.A. Roeloffs, Persistent water level changes in a well near Parkfield, California, due to local and distant earthquakes, J. Geophys. Res. 103 (1998) 869–889.
[3] K. Terzaghi, Theoretical Soil Mechanics, Wiley, New York, 1943, 304 pp.
[4] J.D. Byerlee, Friction of rocks, Pure Appl. Geophys. 116 (1978) 615–626.
[5] R.H. Sibson, Implication of fault-valve behavior for rupture nucleation and recurrence, Tectonophysics 211 (1992) 283–293.
[6] R.C. Briggs, H.C. Troxell, Effect of Arvin-Tehachapi earthquake on spring and stream flow, in earthquakes in Kern County, California during 1952, Bull. Calif. Div. Mines 171 (1955) 81–98.
[7] R.H. Sibson, High-angle reverse faults, fluid pressure cycling, and mesothermal gold-quartz deposits, Geology 16 (1988) 551–555.
[8] S.F. Cox, Faulting processes at high fluid pressures: An example of fault valve behavior from Wattle Gully Fault, Victoria, Australia, J. Geophys. Res. 100 (1995) 12841–12859.
[9] P.T. Nguyen, S.F. Cox, L.B. Harris, C.M. Powell, Fault-valve behavior in optimally oriented shear zones: an example at the Revenge gold mine, Kambalda, Western Australia, J. Struct. Geol. 20 (1998) 1625–1640.
[10] W.J. Bosl, A. Nur, Crustal fluids and earthquakes, in: J.B. Rundle, D.L Turcotte, W. Klein (Eds.), GeoComplexity and the Physics of Earthquakes, Geophys. Monogr. 120, 2000, pp. 267–284.
[11] G.E. Andreasen, J.W. Brookhart, Reverse water-level fluctuations, in: R. Bentall (Ed.), Methods of Collecting

and Interpreting Ground-Water Data, U.S. Geol. Surv. Water-Supply Pap. 1544-H, 1963, pp. 30–35.
[12] A. Verruijt, Elastic storage of aquifers, in: R.J.M. DeWiest (Ed.), Flow through Porous Media, Academic Press, New York, 1969, pp. 331–376.
[13] R.G. Wolff, Relationship between horizontal strain near a well and reverse water level fluctuation, Water Resour. Res. 6 (1970) 1721–1728.
[14] J.D. Rodrigues, The Noordbergum effect and characterization of aquitards at the Rio Maior mining project, Ground Water 21 (1983) 200–207.
[15] H.R. Langguth, C. Treskatis, Reverse water level fluctuations in the semiconfined aquifer systems - 'Rhade Effect', J. Hydrol. 109 (1989) 79–93.
[16] J. Mandel, Consolidation des sols, Geotechnique 3 (1953) 287–299.
[17] C.W. Cryer, A comparison of the three-dimensional consolidation theories of Biot and Terzaghi, Q. J. Appl. Math. 16 (1963) 401–412.
[18] R.L. Schiffman, A.T. Chen, J.C. Jordan, An analysis of consolidation theories, J. Soil Mech. Found. Div. SM1 (1969) 285–312.
[19] R.W. Lewis, B.A. Schrefler, The Finite Element Method in the Deformation and Consolidation of Porous Media, Wiley, New York 1987, 344 pp.
[20] P.A. Hsieh, Deformation-induced changes in hydraulic head during ground-water withdrawal, Ground Water 34 (1996) 1082–1089.
[21] J.-M. Kim, R.R. Parizek, Numerical simulation of the Noordbergum effect resulting from groundwater pumping in a layered aquifer system, J. Hydrol. 202 (1997) 231–243.
[22] M.A. Biot, General theory of three-dimensional consolidation, J. Appl. Phys. 12 (1941) 155–164.
[23] H.F. Wang, Theory of Linear Poroelasticity with Applications to Geomechanics and Hydrogeology, Princeton University Press, 2000, 287 pp.
[24] E. Stanislavsky, G. Garven, The minimum depth of fault failure in compressional environments, Geophys. Res. Lett. 29 (2002) 10.1029/2002GL016363.
[25] R.A. Freeze, J.A. Cherry, Groundwater, Prentice-Hall, Englewood Cliffs, NJ, 1979, 604 pp.
[26] E. Detournay, A.H.D. Cheng, Fundamentals of poroelasiticity, in: J.A. Hudson (Ed.), Comprehensive Rock Engineering; Principles, Practice and Projects II, Pergamon Press, Oxford, 1993, pp. 113–171.
[27] S.E. Ingebritsen, C.E. Manning, Geological implications of a permeability-depth curve for the continental crust, Geology 27 (1999) 1107–1110.
[28] R.E. Wallace, H.T. Morris, Characteristics of faults and shear zones in deep mines, Pure Appl. Geophys. 124 (1986) 107–125.
[29] J.S. Caine, C.B. Forster, Fault zone architecture and fluid flow: Insights from field data and numerical modeling, in: W.C. Haneberg, P.S Mozley, J.C. Moore, L.B. Goodwin (Eds.), Faults and Subsurface Fluid Flow in the Shallow Crust, AGU Monogr. 113 (1999) 101–127.
[30] D.F. McTigue, Thermoelastic response of fluid-saturated porous rock, J. Geophys. Res. 91 (1986) 9533–9542.
[31] M. Antonellini, A. Aydin, Effects of faulting on fluid flow in porous sandstones: petrophysical properties, AAPG Bull. 78 (1994) 355–377.
[32] M.K. Hubbert, W.W. Rubey, Role of fluid pressure in mechanics of overthrust faulting, Geol. Soc. Am. Bull. 70 (1959) 115–206.
[33] F.A.F. Berry, High fluid potentials in the California Coast Ranges and their tectonic significance, AAPG Bull. 57 (1973) 1219–1249.
[34] W.S. Fyfe, N.J. Price, A.B. Thompson, Fluids in the Earth's Crust, Elsevier, Amsterdam, 1978.
[35] J.C. Moore, P. Vrolijk, Fluids in accretionary prisms, Rev. Geophys. 30 (1992) 113–135.
[36] C.E. Neuzil, Abnormal pressures as hydrodynamic phenomena, Am. J. Sci. 295 (1995) 742–786.
[37] T. Masterlark, C. DeMets, H.F. Wang, O. Sanchez, J. Stock, Homogeneous vs heterogeneous subduction zone models: Coseismic and postseismic deformation, Geophys. Res. Lett. 28 (2001) 4047–4050.
[38] T. Masterlark, H.F. Wang, Transient stress-coupling between the 1992 Landers and 1999 Hector Mine, California, earthquakes, Bull. Seism. Soc. Am. 92 (2002) 1470–1486.
[39] M. Cocco, J.R. Rice, Pore pressure and poroelasticity effects in Coulomb stress analysis of earthquake interactions, J. Geophys. Res. 107 (2002) 10.1029/2000JB000138.
[40] C.A. Morrow, D.E. Moore, D.A. Lockner, Permeability reduction in granite under hydrothermal conditions, J. Geophys. Res. 106 (2001) 30551–30560.
[41] R.S. Stein, C.P. King, J. Lin, Change in failure stress on the southern San Andreas fault system caused by the 1992 magnitude = 7.4 Landers earthquake, Science 258 (1992) 1328–1332.